Physica E 93 (2017) 257–264

Contents lists available at ScienceDirect

Physica E

journal homepage: www.elsevier.com/locate/physe

Vibration analysis of defective graphene sheets using nonlocal elasticity theory

S.F. Asbaghian Namin, R. Pilafkan*

University of Mohaghegh Ardabili, Ardabil, Iran

ARTICLE INFO

Keywords:
Graphene sheet
Defect
Fundamental frequency
Nonlocal elasticity theory
Defect reconstruction

ABSTRACT

Many papers have studied the free vibration of graphene sheets. However, all this papers assumed their atomic structure free of any defects. Nonetheless, they actually contain some defects including single vacancy, double vacancy and Stone-Wales defects. This paper, therefore, investigates the free vibration of defective graphene sheets, rather than pristine graphene sheets, via nonlocal elasticity theory. Governing equations are derived using nonlocal elasticity and the first-order shear deformation theory (FSDT). The influence of structural defects on the vibration of graphene sheets is considered by applying the mechanical properties of defective graphene sheets. Afterwards, these equations solved using generalized differential quadrature method (GDQ). The small-scale effect is applied in the governing equations of motion by nonlocal parameter. The effects of different defect types are inspected for graphene sheets with clamped or simply-supported boundary conditions on all sides. It is shown that the natural frequencies of graphene sheets decrease by introducing defects to the atomic structure. Furthermore, it is found that the number of missing atoms, shapes and distributions of structural defects play a significant role in the vibrational behavior of graphene. The effect of vacancy defect reconstruction is also discussed in this paper.

1. Introduction

Experimental and theoretical studies in the fields of microstructures and nanostructures increased substantially after the synthesis and characterization of carbon nanotubes by Iijima in 1991 [1]. Eventually, with the development of these fields, graphene sheets drew attentions to themselves, because of their unique mechanical, electrical and electronic properties. Nowadays, graphene sheets are widely used in nano-sensors, nano-oscillators, electrical batteries, nano-composites, and nano-electromechanical resonators [2,3]. As a result, investigating the mechanical characteristics of graphene sheets is inevitable.

Among various mechanical characteristics of graphene sheets, their vibrational behavior is of great importance. Due to difficulties in conducting experiments to determine the mechanical properties of graphene sheets, generally analytical methods, numerical modelings, and molecular dynamics simulations are used to determine their vibrational characteristics. Up until now, several studies have been done on the vibration of graphene sheets. Murmu and Pradhan [2] employed an analytical method using the separation of variables to investigate the effect of nonlocal parameter on the vibration of graphene sheets. Pradhan and Phadikar [4] calculated natural frequencies of graphene sheets analytically by modifying the classical laminated plate theory (CLPT) and the first shear deformation theory (FSDT) using nonlocal elasticity theory. Hosseini-Hashemi et al. [5] used the Mindlin theory and introduced some potential and auxiliary functions to study the free vibration of graphene sheets. Zhang et al. [6] implemented an element-free kp-Ritz to investigate the free vibrational behavior of a single-layered graphene sheet (SLGS). Moreover, Zhang et al. [7] used nonlocal elasticity theory and CLPT to study the vibrational behavior of bilayer graphene sheets (BLGSs) in a magnetic field.

Zhang et al. [8] also analyzed nonlinear large deformation of SLGSs using an element-free kp-Ritz. Zhang et al. [9] studied the transient analysis of SLGSs via an element-free kp-Ritz method. Ansari et al. [10] implemented the finite element method (FEM) to analyze the free vibration of multi-layered graphene sheets. Ansari et al. [11] investigated the vibration of single-layered graphene sheets (SLGSs) using a nonlocal continuum plate model and then validated the calculated results with ones obtained by the molecular dynamics simulations. Pradhan and Kumar [12] studied the small-scale effect on the vibration analysis of orthotropic SLGSs. They employed the differential quadrature method (DQM) to solve governing equations derived using the nonlocal elasticity theory. Xing and Liu [13] found exact solutions for

* Corresponding author.
E-mail address: rezapilafkan@uma.ac.ir (R. Pilafkan).

http://dx.doi.org/10.1016/j.physe.2017.06.014
Received 13 March 2017; Received in revised form 8 May 2017; Accepted 16 June 2017
Available online 17 June 2017

the free vibration of thin orthotropic rectangular plates. This problem solved for various boundary conditions and validated with results obtained by FEM. Setoodeh and Malekzadeh [14] investigated the free vibration analysis of orthotropic SLGSs using the nonlocal Mindlin plate theory and employing the DQM.

On the other hand, graphene sheets are assumed perfect, i.e. without any defects, in the aforesaid papers. Nonetheless, mass production of perfect graphene sheets can be a formidable task [15]; hence, structural defects do exist in graphene, like in any other real material [16]. Researches have showed that even a small number of defects in the atomic structure can deteriorate the mechanical and electronic properties of graphene materials [17]. Furthermore, defective graphene sheets can be useful in some applications. For instance, they enable scientists to tailor the local properties of graphene and to achieve new functionalities [16]. Therefore, the investigation of mechanical and electrical properties of graphene sheets seems necessary.

The mechanical and electrical properties of graphene materials including Young's modulus, fracture strength, and electrical conductivity have been studied so far. For instance, Jing et al. [15] investigated the effect of defects such as vacancy and Stone-Wales defects on the Young's modulus of graphene sheets via molecular dynamics. Xiao et al. [17] employed an atomistic based finite bond element model for the prediction of fracture and progressive failure of graphene sheets and carbon nanotubes. Xiao et al. [18] used the same method to investigate the tensile behavior of graphene sheets and carbon nanotubes with multiple Stone-Wales defects. Wang et al. [19] utilized molecular dynamics simulations to study the fracture of graphene sheets with vacancies and Stone-Wales defects at different temperatures. Ansari et al. [20] studied the effects of two main types of structural defects, i.e. Stone-Wales and single vacancy, on the mechanical properties of single-layered graphene sheets (SLGSs). Banhart et al. [16] reviewed the various structural defects in graphene. However, the effect of structural defects on the vibrational behavior of graphene sheets has not yet been investigated.

The structural defects can be introduced to graphene sheets by either material production process or chemical treatment [15,16]. They generally can be classified into three categories: incomplete bonding defects, topological defects, and heterogeneous defects [15]. In this work, for the first time, the atomic structures of graphene sheets used in the vibration analysis are considered defective rather than perfect. In other words, the effects of Stone-Wales (SW), single vacancy (SV), and double vacancy (DV) defects on the free vibration of SLGSs are studied. On the other hand, local continuum modeling can successfully explain and predict physical phenomena at the macro-scale level; nevertheless, its application in nano-scale remains questionable because the applicability of classical field theories is correlated with length scales and for accurate prediction of the mechanical behavior of nanomaterials the small scale effect must be taken into account. As a result, usually, the nonlocal elasticity theory is used in modeling the structures at nano-scale instead of classical elasticity theory [21]. Hence, in this work, the nonlocal elasticity theory and the first-order shear deformation theory are employed to obtain the governing equations. The mechanical properties of defective graphene sheets are applied to the equations in order to consider the influence of defects on the vibration of SLGSs. Subsequently, the governing equations are written in GDQ form and then solved using GDQ method; as a result, the natural frequencies corresponding to the different boundary conditions and defect types are calculated and compared with each other to indicate the effect of various types of defects on the vibration of SLGSs. Finally, free vibrations of SLGSs with reconstructed defects are investigated.

2. Nonlocal plate governing equations

As mentioned in the previous section, the FSDT is used in order to establish governing equations. In this theory, both shear deformations and rotational inertia are taken into account. As a result, despite CLPT, transverse normals (i.e., straight lines perpendicular to the midsurface) do not remain perpendicular to the midsurface after deformation [22]. Fig. 1 shows the coordinate system for the SLGS. As shown in the figure, $z = 0$ plane is the middle plane of the SLGS. Considering FSDT, displacement field for the plate can be expressed as [22]:

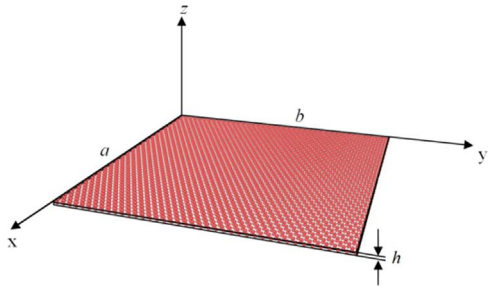

Fig. 1. Coordinate system for SLGS.

$$u_x(x, y, z, t) = u(x, y, t) + z\psi_x(x, y, t) \tag{1}$$

$$u_y(x, y, z, t) = v(x, y, t) + z\psi_y(x, y, t) \tag{2}$$

$$u_z(x, y, z, t) = w(x, y, t) \tag{3}$$

Where u_x, u_y and u_z are displacements of an arbitrary point on $z = 0$ plane in x, y and z directions and u, v, w are displacements of an arbitrary point (x, y, z) in x, y and z directions, respectively. Additionally, ψ_x, ψ_y are rotations about x, y Axis, respectively.

The strains are obtained as follows [22]:

$$\begin{Bmatrix} \varepsilon_{xx} \\ \varepsilon_{yy} \\ \varepsilon_{xy} \end{Bmatrix} = \begin{Bmatrix} \frac{\partial u}{\partial x} \\ \frac{\partial v}{\partial y} \\ \frac{1}{2}\left(\frac{\partial u}{\partial y} + \frac{\partial v}{\partial x}\right) \end{Bmatrix} + z \begin{Bmatrix} \frac{\partial \psi_x}{\partial x} \\ \frac{\partial \psi_y}{\partial y} \\ \frac{1}{2}\left(\frac{\partial \psi_x}{\partial x} + \frac{\partial \psi_y}{\partial y}\right) \end{Bmatrix} \tag{4}$$

$$\begin{Bmatrix} \varepsilon_{xz} \\ \varepsilon_{yz} \end{Bmatrix} = \begin{Bmatrix} \frac{1}{2}\left(\psi_x + \frac{\partial w}{\partial x}\right) \\ \frac{1}{2}\left(\psi_y + \frac{\partial w}{\partial y}\right) \end{Bmatrix} \tag{5}$$

ε_{xx}, ε_{yy}, ε_{zz} and ε_{xy}, ε_{xz}, ε_{yz} denote normal and shear strain tensor components, respectively. It should be noted that $\varepsilon_{zz} = 0$, because it was assumed that the transverse normals are inextensible.

Furthermore, based on nonlocal elasticity theory stress at any point in a continuum is a function of strain at all points of the continuum [23]. Accordingly, the constitutive relation in the small scales is written as follows [4]:

$$(1 - \mu\nabla^2)\sigma = t \tag{6}$$

Where σ is nonlocal stress tensor, t is local stress tensor, and μ denotes the nonlocal parameter.

Using Eq. (6) and based on the FSDT, one can obtain a relation between the nonlocal stresses and strains for an isotropic plate [24]:

$$\begin{Bmatrix} \sigma_{xx} \\ \sigma_{yy} \\ \sigma_{xy} \end{Bmatrix} - \mu\nabla^2 \begin{Bmatrix} \sigma_{xx} \\ \sigma_{yy} \\ \sigma_{xy} \end{Bmatrix} = \begin{bmatrix} E/(1-\upsilon^2) & \upsilon E/(1-\upsilon^2) & 0 \\ \upsilon E/(1-\upsilon^2) & E/(1-\upsilon^2) & 0 \\ 0 & 0 & 2G \end{bmatrix} \begin{Bmatrix} \varepsilon_{xx} \\ \varepsilon_{yy} \\ \varepsilon_{xy} \end{Bmatrix} \tag{7}$$

$$\begin{Bmatrix} \sigma_{xz} \\ \sigma_{yz} \end{Bmatrix} - \mu\nabla^2 \begin{Bmatrix} \sigma_{xz} \\ \sigma_{yz} \end{Bmatrix} = \begin{bmatrix} 2G & 0 \\ 0 & 2G \end{bmatrix} \begin{Bmatrix} \varepsilon_{xz} \\ \varepsilon_{yz} \end{Bmatrix} \tag{8}$$

Where E, G and υ are the young modulus, the shear modulus, and the poisson's ratio, respectively.

On the other hand, the principle of virtual work can be applied to derive the equilibrium equations of the SLGS [4]. Following governing equations are obtained, using the principle of virtual work [4]:

$$\frac{\partial N_{xx}}{\partial x} + \frac{\partial N_{xy}}{\partial y} = I_1 \frac{\partial^2 u}{\partial t^2} \tag{9}$$

$$\frac{\partial N_{xy}}{\partial x} + \frac{\partial N_{yy}}{\partial y} = I_1 \frac{\partial^2 v}{\partial t^2} \tag{10}$$

$$\frac{\partial Q_{xx}}{\partial x} + \frac{\partial Q_{yy}}{\partial y} + q + \{\frac{\partial}{\partial x}(N_{xx}\frac{\partial w}{\partial x}) + \frac{\partial}{\partial y}(N_{yy}\frac{\partial w}{\partial y}) + \frac{\partial}{\partial x}(N_{xy}\frac{\partial w}{\partial y}) + \frac{\partial}{\partial y}(N_{xy}\frac{\partial w}{\partial x})\} = I_1 \frac{\partial^2 w}{\partial t^2} \tag{11}$$

$$\frac{\partial M_{xx}}{\partial x} + \frac{\partial M_{xy}}{\partial y} - Q_{xx} = I_3 \frac{\partial^2 \psi_x}{\partial t^2} \tag{12}$$

$$\frac{\partial M_{xy}}{\partial x} + \frac{\partial M_{yy}}{\partial y} - Q_{yy} = I_3 \frac{\partial^2 \psi_y}{\partial t^2} \tag{13}$$

Where N_{xx}, N_{xy}, N_{yy}, M_{xx}, M_{xy}, M_{yy}, Q_{xx} and Q_{yy} denote stress resultants, which are defined as follows:

$$N_{xx} = \int_{-h/2}^{h/2} \sigma_{xx} dz, N_{xy} = \int_{-h/2}^{h/2} \sigma_{xy} dz, N_{yy} = \int_{-h/2}^{h/2} \sigma_{yy} dz \tag{14}$$

$$M_{xx} = \int_{-h/2}^{h/2} z\sigma_{xx} dz, M_{xy} = \int_{-h/2}^{h/2} z\sigma_{xy} dz, M_{yy} = \int_{-h/2}^{h/2} z\sigma_{yy} dz \tag{15}$$

$$Q_{xx} = \int_{-h/2}^{h/2} \sigma_{xz} dz, Q_{yz} = \int_{-h/2}^{h/2} \sigma_{yz} dz \tag{16}$$

Furthermore, I_1 and I_3 are mass moments of inertia and defined as:

$$I_1 = \int_{-h/2}^{h/2} \rho dz, I_3 = \int_{-h/2}^{h/2} \rho h^2 dz \tag{17}$$

Subsequently, (7) and (8) and (14)–(16) can be used to express stress resultants in terms of the displacements:

$$M_{xx} - \mu\nabla^2 M_{xx} = D(\frac{\partial \psi_x}{\partial x} + \upsilon\frac{\partial \psi_y}{\partial y}) \tag{18}$$

$$M_{yy} - \mu\nabla^2 M_{yy} = D(\frac{\partial \psi_y}{\partial y} + \upsilon\frac{\partial \psi_x}{\partial x}) \tag{19}$$

$$M_{xy} - \mu\nabla^2 M_{xy} = \frac{1}{2}(1-\upsilon)D(\frac{\partial \psi_x}{\partial y} + \frac{\partial \psi_y}{\partial x}) \tag{20}$$

$$Q_{xx} - \mu\nabla^2 Q_{xx} = kGh(\frac{\partial w}{\partial x} + \psi_x) \tag{21}$$

$$Q_{yy} - \mu\nabla^2 Q_{yy} = kGh(\frac{\partial w}{\partial y} + \psi_y) \tag{22}$$

In these relations $k = 5/6$ is the shear correction factor.

Finally, using (18)–(22), (11)–(13) expressed in the terms of displacements:

$$kGh(\frac{\partial \psi_x}{\partial x} + \frac{\partial \psi_y}{\partial y} + \frac{\partial^2 w}{\partial x^2} + \frac{\partial^2 w}{\partial y^2}) = I_1(\frac{\partial^2 w}{\partial t^2} - \mu\nabla^2\frac{\partial^2 w}{\partial t^2}) \tag{23}$$

$$D\frac{\partial^2 \psi_x}{\partial x^2} + \frac{(1+\upsilon)}{2}D\frac{\partial^2 \psi_y}{\partial x \partial y} + \frac{1}{2}(1-\upsilon)D\frac{\partial^2 \psi_x}{\partial y^2} - kGh(\frac{\partial w}{\partial x} + \psi_x) = I_3(\frac{\partial^2 \psi_x}{\partial t^2} - \mu\nabla^2\frac{\partial^2 \psi_x}{\partial t^2}) \tag{24}$$

$$\frac{(1+\upsilon)}{2}D\frac{\partial^2 \psi_x}{\partial x \partial y} + D\frac{\partial^2 \psi_y}{\partial y^2} + \frac{1}{2}(1-\upsilon)D\frac{\partial^2 \psi_y}{\partial x^2} - kGh(\frac{\partial w}{\partial y} + \psi_y) = I_3(\frac{\partial^2 \psi_y}{\partial t^2} - \mu\nabla^2\frac{\partial^2 \psi_y}{\partial t^2}) \tag{25}$$

It should be mentioned that (9), (10) and the terms including q, N_{xx}, N_{xy} and N_{yy} were eliminated, because it was assumed that the plate is free from any in-plane or transverse loading [4].

3. Solution using generalized differential quadrature method

3.1. Generalized differential quadrature method

Generalized differential quadrature method is a numerical solution technique for solving initial and boundary condition problems of a wide range of engineering applications. It can be used as a convenient alternative to the finite difference and finite element methods due to its great accuracy and capability in solving complicated ordinary and partial differential equations [25]. In summary, in this method N_x and N_y grid points are chosen in x and y directions, then partial derivative of a function with respect to a coordinate (x or y) at a grid point is estimated by weighted linear sum of values of that function in all grid points along that direction. Therefore, rth derivative of function $\varphi(x, y)$ at point $x = x_i$ and in direction $y = y_j$ can be obtained using the following relation:

$$\left.\frac{\partial^r \varphi}{\partial x^r}\right|_{x=x_i} = \sum_{k=1}^{N_x} A_{ik}^{(r)} \varphi_{kj} \tag{26}$$

Similarly, one can write:

$$\left.\frac{\partial^s \varphi}{\partial y^s}\right|_{y=y_i} = \sum_{l=1}^{N_y} B_{jm}^{(s)} \varphi_{im} \tag{27}$$

Where $A_{ik}^{(r)}$ and $B_{jm}^{(s)}$ are weighting coefficients and $\varphi_{ij} = \varphi(x_i, y_j)$.

The weighting coefficients of the first derivatives are obtained from:

$$A_{ik}^{(1)} = \frac{\prod_{v=1, v\neq i}^{N_x}(x_i - x_v)}{(x_i - x_k)\prod_{v=1, v\neq k}^{N_x}(x_k - x_v)}; \; k, i = 1, ..., N_x, \; k \neq i \tag{28}$$

Furthermore, the weighting coefficients of higher-order derivatives are determined by:

$$A_{ik}^{(r)} = \begin{cases} r\left[A_{ii}^{(r-1)}A_{ik}^{(1)} - \frac{A_{ik}^{(r-1)}}{x_i - x_k}\right], \; i \neq k \\ A_{ii}^{(r)} = -\sum_{v=1, v\neq i}^{N_x} A_{iv}^{(r)}, \; i = k \end{cases}$$
$$(i, j = 1, 2, 3, ..., N_x; \; 2 \leq r \leq N_x - 1) \tag{29}$$

3.2. GDQ form of governing equations

To solve (23)–(25) using GDQ technique, these equations should be rewritten in GDQ form. Since w, ψ_x and ψ_y were assumed as the periodic functions, one can write:

$$x = aX, \; y = bY \tag{30}$$

$$w = hWe^{j\omega t}, \; \psi_x = \Psi_x e^{j\omega t}, \; \psi_y = \Psi_y e^{j\omega t} \tag{31}$$

Eventually, using (26)–(29) and substituting (30) and (31) in (23)–(25) the following analogous equations can be obtained:

$$kGh(\frac{h}{a^2}\sum_{k=1}^{N_x} A_{ik}^{(2)} W_{kj} + \frac{1}{a}\sum_{k=1}^{N_x} A_{ik}^{(1)} \Psi_{xkj} + \frac{h}{b^2}\sum_{m=1}^{N_y} B_{jm}^{(2)} W_{im} + \frac{1}{b}\sum_{m=1}^{N_y} B_{jm}^{(1)} \Psi_{y_{im}}) = -\omega^2[I_1 W_{ij} - \mu I_1(\frac{1}{a^2}\sum_{k=1}^{N_x} A_{ik}^{(2)} W_{kj} + \frac{1}{b^2}\sum_{m=1}^{N_y} B_{jm}^{(2)} W_{im})] \tag{32}$$

$$\frac{D}{a^2}\sum_{k=1}^{N_x} A_{ik}^{(2)} \Psi_{x_{kj}} + \frac{(1+\upsilon)}{2}\frac{D}{ab}\sum_{k=1}^{N_x}\sum_{m=1}^{N_y} A_{ik}^{(2)} B_{jm}^{(2)} \Psi_{y_{km}} + \frac{1}{2}(1-\upsilon)\frac{D}{b^2}\sum_{m=1}^{N_y} B_{jm}^{(2)} \Psi_{x_{im}} = -\omega^2[I_3 W_{ij} - \mu I_3(\frac{1}{a^2}\sum_{k=1}^{N_x} A_{ik}^{(2)} \Psi_{x_{kj}} + \frac{1}{b^2}\sum_{m=1}^{N_y} B_{jm}^{(2)} \Psi_{x_{im}})] \tag{33}$$

$$\frac{D}{b^2}\sum_{m=1}^{N_y} B_{jm}^{(1)}\Psi_{y_{im}} + \frac{(1+\upsilon)}{2}\frac{D}{ab}\sum_{k=1}^{N_x}\sum_{m=1}^{N_y} A_{ik}^{(2)} B_{jm}^{(2)}\Psi_{x_{km}} +$$
$$\frac{1}{2}(1-\upsilon)\frac{D}{a^2}\sum_{k=1}^{N_x} A_{ik}^{(2)}\Psi_{y_{kj}} = -\omega^2[I_3 W_{ij} - \mu I_3(\frac{1}{a^2}\sum_{k=1}^{N_x} A_{ik}^{(2)}\Psi_{y_{kj}} +$$
$$\frac{1}{b^2}\sum_{m=1}^{N_y} B_{jm}^{(2)}\Psi_{y_{im}})];$$
$$i = 1, 2, ..., N_x, j = 1, 2, ..., N_y \quad (34)$$

3.3. Boundary conditions

In order to solve equation, applying the appropriate boundary conditions is necessary. For the *all edges clamped* (CCCC) boundary conditions, in which (C) refers to the clamped boundary conditions one can write:

$$X = 0, 1;\ W = \Psi_x = \Psi_y = 0$$
$$Y = 0, 1;\ W = \Psi_x = \Psi_y = 0 \quad (35)$$

The GDQ form of boundary conditions:

$$i = 1, N_x;\ W_{ij} = \Psi_{x_{ij}} = \Psi_{y_{ij}} = 0$$
$$j = 1, N_y;\ W_{ij} = \Psi_{x_{ij}} = \Psi_{y_{ij}} = 0 \quad (36)$$

For the all edges simply supported (SSSS) boundary conditions, in which (S) refers to the simply supported boundary conditions the following relations applied:

$$X = 0, 1;\ W = \Psi_y = 0,\ M_{xx} = 0$$
$$Y = 0, 1;\ W = \Psi_x = 0,\ M_{yy} = 0 \quad (37)$$

The GDQ form of boundary conditions:

$$i = 1, N_x;\ W_{ij} = \Psi_{y_{ij}} = 0;$$
$$D\sum_{k=1}^{N_x} A_{ik}^{(1)}\Psi_{x_{kj}} + \upsilon D\sum_{m=1}^{N_y} B_{jm}^{(1)}\Psi_{y_{im}} = 0$$
$$j = 1, N_y;\ W_{ij} = \Psi_{x_{ij}} = 0;$$
$$\upsilon D\sum_{k=1}^{N_x} A_{ik}^{(1)}\Psi_{x_{kj}} + D\sum_{m=1}^{N_y} B_{jm}^{(1)}\Psi_{y_{im}} = 0 \quad (38)$$

3.4. Eigenvalue problem

Assembling (32)-(38) into an eigenvalue problem is the final step in the GDQ solution procedure. This eigenvalue problem can be written as the following matrix form:

$$\begin{bmatrix}[S_{dd}] & [S_{db}]\\ [S_{bd}] & [S_{bb}]\end{bmatrix}_{(N\times N)}\begin{Bmatrix}\delta_d\\ \delta_b\end{Bmatrix}_{(N)} = \begin{Bmatrix}\{\omega^2[M_{dd}]\{\delta_d\}\}\\ \{0\}\end{Bmatrix}_{(N)} \quad (39)$$

Where $[S_{dd}]$, $[S_{db}]$, $[S_{bd}]$and$[S_{bb}]$ are the coefficient matrices of the left hand side of (32)-(34) in which the subscript $b$and$d$ refer to the boundary and domain, respectively. $[M_{dd}]$ is the coefficient matrix of the right hand side of (32)-(34).$\{\delta_d\}$and$\{\delta_b\}$ are the displacement vectors corresponding to the domain and boundary grid points.

Eigenvalues (i.e. natural frequencies,ω) and eigenvectors of (39) are calculated using the condensation technique as follows [7]:

$$[M_{dd}^{-1}]([S_{dd}] - [S_{db}][S_{bb}^{-1}][S_{bd}])\{\delta_d\} - \omega^2[I][\delta_d] = 0 \quad (40)$$

4. Results and discussion

4.1. Effect of common structural defects on natural frequencies of graphene sheets

In this research, for the first time, the effect of the most common defects, including SV, DV, and SW defects, on the natural frequencies of graphene sheets were studied. The SV and DV defects can be created by removing one carbon atom and two neighboring atoms from a pristine graphene sheet, respectively [15]. These defects are shown in Fig. 2(a) and (b). The SW defect does not involve any removed or added atom. In fact, it is formed by rotating a C-C bond by 90° and consequently, transforming four hexagons into two pentagons and two heptagons (SW (55–77)), as shown in Fig. 2(c) [16].

The graphene sheet is assumed isotopic in this work. Introducing defects into graphene sheets merely influences its mechanical properties, especially its Young's modulus, rather than the governing equation. Thus, in this paper, the effect of defects is considered in the governing equations via Young's modulus. The Young's modulus and Poisson's ratio of the pristine graphene sheet are considered 1.032TPa, 00.3, respectively [4,15]. Also, the thickness of each plate and the density of the graphene are assumed $h = 0.34$nm and $\rho = 2300\ \mathrm{kg/m^3}$. Values of Young's modulus for various defective graphene sheets are obtained by Jing et al. [15]. These values are used in this paper. In order to employ the Young's moduli provided by Jing et al. [15] properly, the side lengths of graphene sheets are considered 5.823nmand50.904 nm, respectively.

The convergence study and the validation of GDQ method are conducted for a perfect SLGS (i.e. SLGS with no defects), since there is no previous data available for the natural frequencies of defective graphene sheets. First, the convergence study for the GDQ technique is conducted. To achieve this goal, the fundamental frequency is calculated for a square pristine SLGS with side length of 10 nm and SSSS boundary conditions for both local ($\mu = 0$) and nonlocal ($\mu = 1\,(\mathrm{nm})^2$) assumptions. Table 1 shows the fundamental frequencies for various number of grid points chosen along each axis. It can be noted from Table 1 that after employing 11 grid points results converge and there is no need for further increasing in the number of grid points.

Subsequently, the natural frequencies obtained in present work using the GDQ method for both local and nonlocal plate are listed in Table 2 and compared with exact solutions [4]. They are acquired for a square isotropic pristine SLGS with 10 nm side length and all edges simply supported boundary conditions. From this table, one could find that present results are in good agreement with those of the exact solution [4].

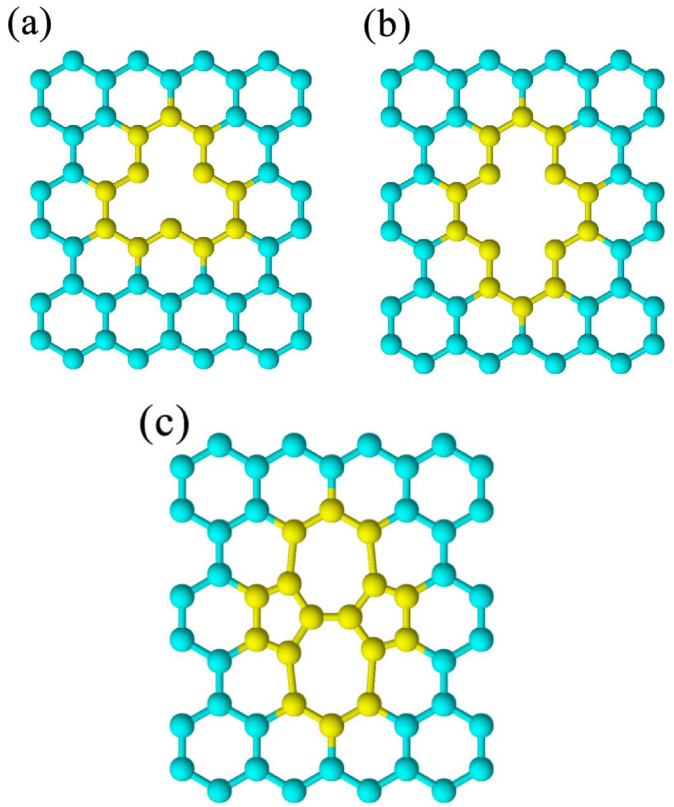

Fig. 2. Structural defects in graphene sheets (a) SV defect (b) DV defect (c) SW defect (55–77).

Table 1
Convergence study of fundamental frequencies (THz) for the GDQ method.

Number of grid points	local (μ=0)	nonlocal (μ=1)
7	0.0624	0.0684
9	0.0623	0.0682
11	0.0623	0.0682
13	0.0623	0.0682
15	0.0623	0.0682

The nonlocal parameter plays an eminent role in the calculation of natural frequencies for a small graphene sheet based on the nonlocal elasticity theory. Hence, in order to implement nonlocal elasticity theory, determining this parameter is inevitable. Ansari et al. [11] proposed an optimization technique to determine the value of nonlocal parameter. Using this method they proposed 1.41 and 0.87 for SLGSs with SSSS and CCCC boundary conditions, respectively [11]. These values are suggested for pristine graphene sheets. However, there is no such data available for defective graphene sheets. As a result, in this paper, these values will be used as approximate values to calculate the natural frequencies via nonlocal elasticity theory and observe the effect of defects on vibrational behavior of graphene sheets.

First natural frequencies of graphene sheets with SSSS boundary conditions and SV, DV, and SW defects, which are obtained using the nonlocal elasticity, were compared in Fig. 3. The defect degree of vacancies is defined as the density of atoms removed from the pristine graphene sheets. On the other hand, for SW dislocation, it is defined as the density of defected atoms (each SW defect includes two defected atoms). It can be seen that the value of fundamental frequency decreases by introducing any type of defect into the perfect graphene sheet. Additionally, as expected, increasing the defect degree leads to the reduction of the fundamental frequency. However, the influence of defect degree is far more obvious for SV and DV defects. Furthermore, the fundamental frequency of graphene with SV defect is much smaller than that of graphene with DV defect, for the same value of defect degree, since it has more dangling bonds. The same behavior can be observed for CCCC boundary conditions, as shown in Fig. 4.

The effects of various defect types on the natural frequencies of graphene sheets with SSSS and CCCC boundary conditions (corresponding to different mode sequences) are displayed in Figs. 5 and 6. These figures indicate that defects affect all natural frequencies of graphene sheets in a similar way. In fact, all natural frequencies decrease. Besides, SV and DV defects result in a lot more drop in the natural frequencies. Moreover, again, one can observe the same trend for both SSSS and CCCC boundary conditions. Therefore, for the rest of this paper, there is no need to investigate graphene sheets with both SSSS and CCCC boundary conditions; consequently, only graphene sheets with SSSS boundary conditions will be investigated.

In addition, the effects of the number of missing atoms and their distribution are investigated in Fig. 7. As shown in this figure, increasing the number of missing atoms decreases the fundamental frequency of graphene sheets dramatically. Further, one can infer that for the same number of missing atoms, a SV cluster causes more reduction in the fundamental frequency of a SLGS than a DV cluster. Hence, more dispersive missing atoms lead into much lower natural frequencies; therefore, not only the number of missing atoms but also shapes and distributions of the structural defects play a crucial role in how defects affect the fundamental frequency of graphene sheets.

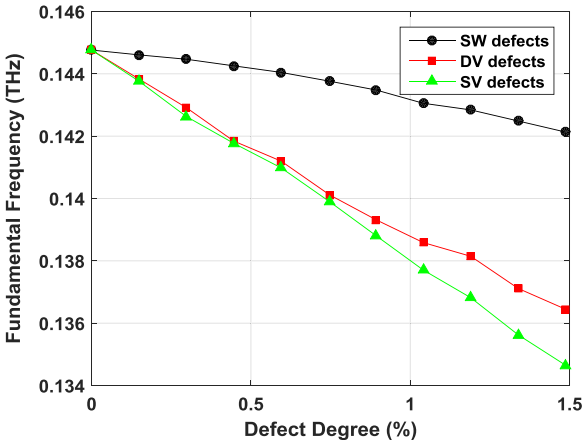

Fig. 3. Effect of defect degree and defect type on the fundamental frequency of graphene sheets with SSSS boundary conditions.

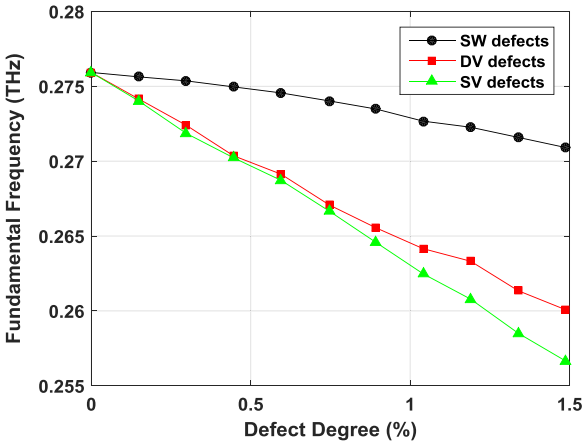

Fig. 4. Effect of defect degree and defect type on the fundamental frequency of graphene sheets with CCCC boundary conditions.

Table 2
Comparison of natural frequencies (THz) using the GDQ method with the exact solution (for a pristine SLGS).

	local			nonlocal		
Mode number	**GDQ**	**Exact (CLPT[4])[a]**	**Exact (FSDT[4])**	**GDQ**	**Exact (CLPT[4])[a]**	**Exact (FSDT[4])**
1	0.0623	0.0625	0.0624	0.0682	0.0684	0.0683
2	0.1384	0.1398	0.1390	0.1695	0.1709	0.1699
3	0.1384	0.1398	0.1390	0.1695	0.1709	0.1699
4	0.2010	0.2041	0.2022	0.2696	0.2730	0.2705
5	0.2371	0.2419	0.2391	0.3356	0.3409	0.3371
6	0.2371	0.2419	0.2391	0.3356	0.3409	0.3371

[a] $\omega_{mn} = \sqrt{(D\left[\left(\frac{m\pi}{a}\right)^2 + \left(\frac{n\pi}{b}\right)^2\right]^2 / (\rho h + \frac{1}{12}\rho h^3[(\frac{m\pi}{a})^2 + (\frac{n\pi}{b})^2])(1 + \mu[(\frac{m\pi}{a})^2 + (\frac{n\pi}{b})^2])}$.

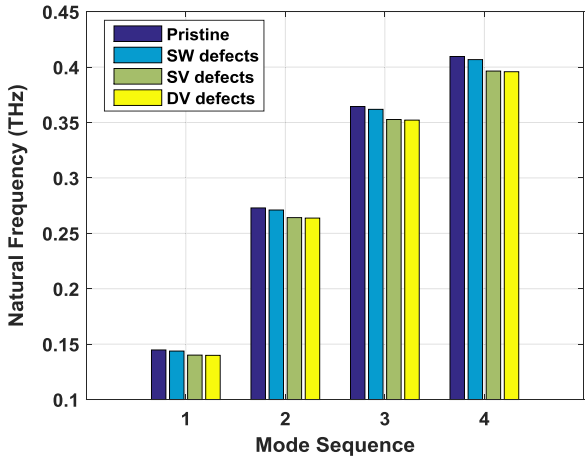

Fig. 5. Effect of various defects on the natural frequencies of graphene sheets with SSSS boundary conditions.

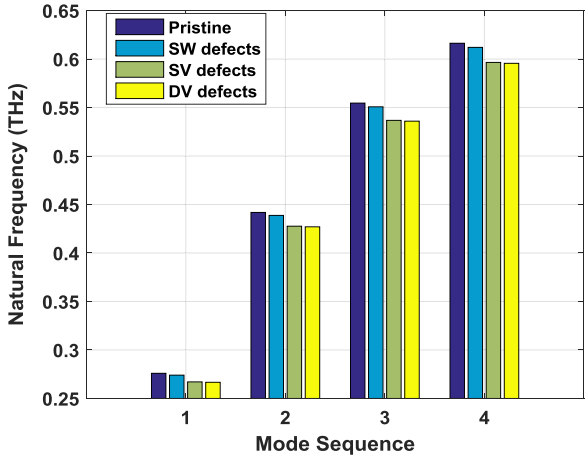

Fig. 6. Effect of various defects on the natural frequencies of graphene sheets with CCCC boundary conditions.

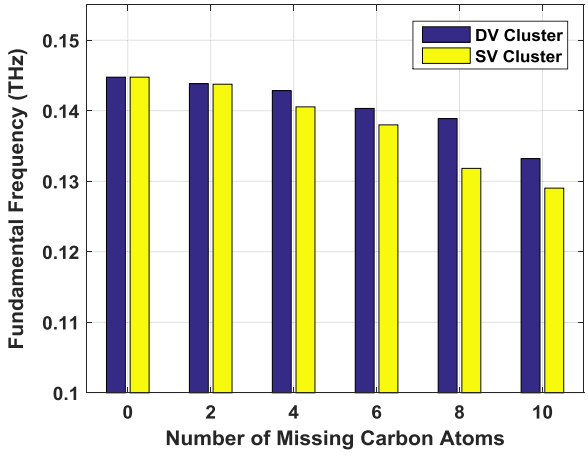

Fig. 7. Effect of number missing atoms and their distribution on fundamental frequency of graphene sheets.

4.2. *Effect of vacancy defect reconstruction on natural frequencies of graphene sheets*

Even though, the structures shown in the Fig. 2 are the initial atomic structures of single and double vacancy defects in graphene sheets they do not have the lowest potential energy. Thus, the lattice may relax into a lower energy state by vacancy defect reconstruction, which includes changing the bonding geometry [15]. This phenomenon has been reported on carbon nanotubes [26]. Since graphene and carbon nanotube have similar structures, one can suppose that this reconstruction will occur in graphene sheets too [11]. This behavior in graphene sheets has been also studied theoretically by El-Barbary et al. [27] and Lee et al. [28]. The SV undergoes a Jahn-Teller distortion, which results in the saturation of two of the three dangling bonds toward the missing atom; the number of dangling bonds reduces to one. As a result, a pentagon and a nonagon (nine-membered ring) are formed (V1 (5–9)), as shown in Fig. 8(a) [16]. Similarly, double vacancy defects may transform to three more stable reconstructed defects, which contain far less dangling bonds.

The fundamental frequencies of graphene sheets with single and double vacancy defects and their reconstructed forms are compared in Figs. 9 and 10. As seen in Fig. 9, reconstruction increases the fundamental frequency of graphene sheets with SV defects; nevertheless, the frequency is still much lower than that of a perfect graphene. It is because of the

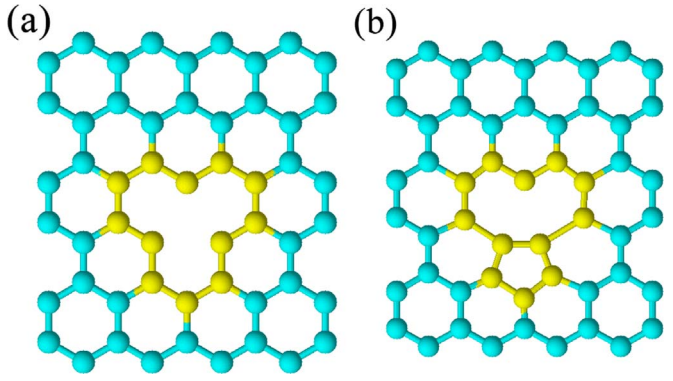

Fig. 8. Atomic structures of SV defects before and after reconstruction in graphene (a) single vacancy (b) reconstructed SV (V1(5–9)).

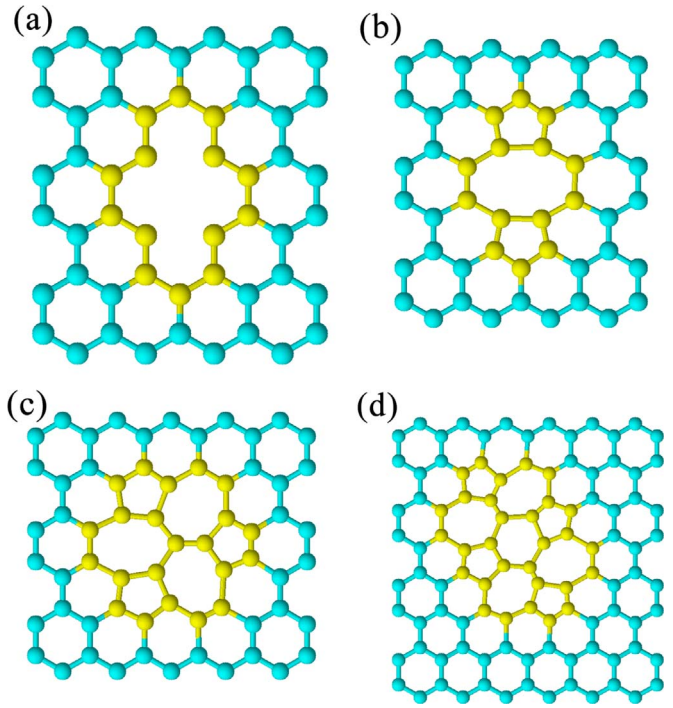

Fig. 9. Atomic structures of DV defects before and after reconstruction in graphene (a) double vacancy (b) reconstructed DV V2(5-8-5) (c) reconstructed DV V2(555–777) (d) reconstructed DV V2(5555-6-7777).

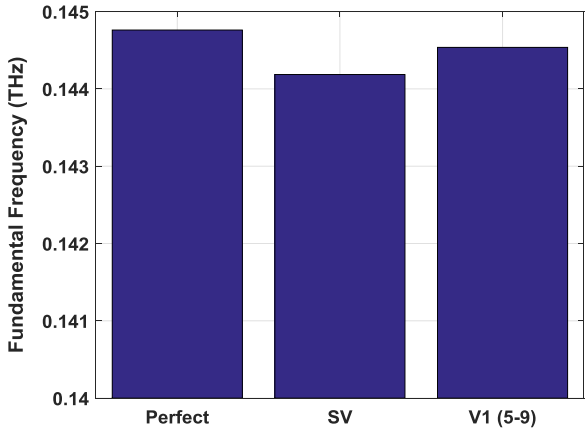

Fig. 10. Comparison of the fundamental frequencies of SLGSs with SV and reconstructed SV defects.

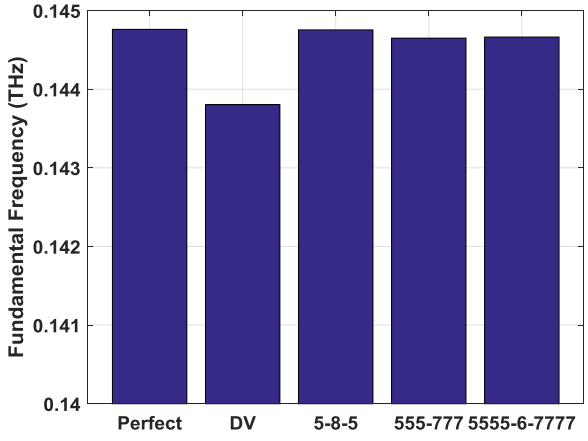

Fig. 11. Comparison of the fundamental frequencies of SLGSs with DV and reconstructed DV defects.

existence of dangling bonds in this reconstructed structure. On the other hand, the reconstruction of the DV defects increases the fundamental frequency of graphene sheets too; however, since there are no dangling bonds in the reconstructed defects, this frequency is really close to that of a pristine graphene (Fig. 11).

5. Conclusion

For the first time, a free vibration analysis of defective graphene sheets was performed using the nonlocal elasticity theory. Since there is no previous data available for the natural frequencies of defective graphene sheets, validation of GDQ method for this case is investigated using pristine graphene sheets, on which no defects present. It is shown that for perfect graphene sheets, the fundamental frequencies obtained by nonlocal elasticity theory are in good agreement with those reported in the literature. The effect of the most typical defects, i.e. SV, DV, and SW, on the vibrational characteristics of graphene sheets was studied. It was observed that SLGSs with all types of defects have lower natural frequencies compared to perfect SLGSs. In addition, the natural frequencies reduce notably by increasing the defect degree; however, this phenomenon is much more obvious for SLGSs with SV and DV defects. Moreover, the fundamental frequency of graphene sheets with SV defects is much smaller than that of graphene sheets with DV defects, for the same value of defect degree, since they have more dangling bonds.

Additionally, the effects of the number of missing atoms and their distribution were investigated. It was shown that increasing the number of missing atoms result in decreasing the natural frequencies of graphene sheets. Further, for the same number of missing atoms, one can infer that SV clusters cause more reduction in the fundamental frequencies of SLGSs than DV clusters. Therefore, it was indicated that not only the number of missing atoms but also shapes and distributions of the structural defects play a key role in how defects affect the natural frequencies of graphene sheets.

Lastly, the effect of vacancy defect reconstruction on natural frequencies of graphene sheets was investigated. It was shown that, the reconstruction increases the fundamental frequencies of graphene sheets with either SV or DV defects. Even though the obtained frequency for the SLGS with the reconstructed SV defect is still far smaller than that of the perfect graphene, this frequency is really close to that of the pristine graphene for SLGSs with the reconstructed DV defects.

References

[1] J. Ramsden, Nanotechnology: An Introduction, Elsevier, 2011.
[2] T. Murmu, S.C. Pradhan, Small-scale effect on the free in-plane vibration of nanoplates by nonlocal continuum model, Phys. E: Low.-Dimens. Syst. Nanostruct. 41 (8) (2009) 1628–1633.
[3] R.H. Baughman, A.A. Zakhidov, W.A. De Heer, Carbon nanotubes–the route toward applications, Science 297 (5582) (2002) 787–792.
[4] S.C. Pradhan, J.K. Phadikar, Nonlocal elasticity theory for vibration of nanoplates, J. Sound Vib. 325 (1) (2009) 206–223.
[5] S. Hosseini-Hashemi, M. Zare, R. Nazemnezhad, An exact analytical approach for free vibration of Mindlin rectangular nano-plates via nonlocal elasticity, Compos. Struct. 100 (2013) 290–299.
[6] R. Ansari, R. Rajabiehfard, B. Arash, Nonlocal finite element model for vibrations of embedded multi-layered graphene sheets, Comput. Mater. Sci. 49 (4) (2010) 831–838.
[7] Y. Zhang, Z.X. Lei, L.W. Zhang, K.M. Liew, J.L. Yu, Nonlocal continuum model for vibration of single-layered graphene sheets based on the element-free kp-Ritz method, Eng. Anal. Bound. Elem. 56 (2015) 90–97.
[8] Y. Zhang, L.W. Zhang, K.M. Liew, J.L. Yu, Free vibration analysis of bilayer graphene sheets subjected to in-plane magnetic fields, Compos. Struct. 144 (2016) 86–95.
[9] Y. Zhang, L.W. Zhang, K.M. Liew, J.L. Yu, Nonlocal continuum model for large deformation analysis of SLGSs using the kp-Ritz element-free method, Int. J. Non-Linear Mech. 79 (2016) 1–9.
[10] Y. Zhang, L.W. Zhang, K.M. Liew, J.L. Yu, Transient analysis of single-layered graphene sheet using the kp-Ritz method and nonlocal elasticity theory, Appl. Math. Comput. 258 (2015) 489–501.
[11] R. Ansari, S. Sahmani, B. Arash, Nonlocal plate model for free vibrations of single-layered graphene sheets, Phys. Lett. A 375 (1) (2010) 53–62.
[12] S.C. Pradhan, A. Kumar, Vibration analysis of orthotropic graphene sheets using nonlocal elasticity theory and differential quadrature method, Compos. Struct. 93 (2) (2011) 774–779.
[13] Y.F. Xing, B. Liu, New exact solutions for free vibrations of thin orthotropic rectangular plates, Compos. Struct. 89 (4) (2009) 567–574.
[14] A.R. Setoodeh, P. Malekzadeh, A.R. Vosoughi, Nonlinear free vibration of orthotropic graphene sheets using nonlocal Mindlin plate theory, Proc. Inst. Mech. Eng. Part C: J. Mech. Eng. Sci. (2011) (0954406211428997).
[15] N. Jing, Q. Xue, C. Ling, M. Shan, T. Zhang, X. Zhou, Z. Jiao, Effect of defects on Young's modulus of graphene sheets: a molecular dynamics simulation, RSC Adv. 2 (24) (2012) 9124–9129.
[16] F. Banhart, J. Kotakoski, A.V. Krasheninnikov, Structural defects in graphene, ACS Nano 5 (1) (2010) 26–41.
[17] J.R. Xiao, J. Staniszewski, J.W. Gillespie, Fracture and progressive failure of defective graphene sheets and carbon nanotubes, Compos. Struct. 88 (4) (2009) 602–609.
[18] J.R. Xiao, J. Staniszewski, J.W. Gillespie, Tensile behaviors of graphene sheets and carbon nanotubes with multiple Stone–Wales defects, Mater. Sci. Eng.: A 527 (3) (2010) 715–723.
[19] M.C. Wang, C. Yan, L. Ma, N. Hu, M.W. Chen, Effect of defects on fracture strength of graphene sheets, Comput. Mater. Sci. 54 (2012) 236–239.
[20] R. Ansari, S. Ajori, B. Motevalli, Mechanical properties of defective single-layered graphene sheets via molecular dynamics simulation, Superlattices Microstruct. 51 (2) (2012) 274–289.

[21] K.M. Liew, Y. Zhang, L.W. Zhang, Nonlocal elasticity theory for graphene modeling and simulation: prospects and challenges, J. Model. Mech. Mater. 1 (1) (2017) 20160159.
[22] J.N. Reddy, Mechanics of Laminated Composite Plates and Shells: Theory and Analysis, CRC press, 2004.
[23] A.C. Eringen, On differential equations of nonlocal elasticity and solutions of screw dislocation and surface waves, J. Appl. Phys. 54 (9) (1983) 4703–4710.
[24] J.N. Reddy, N.D. Phan, Stability and vibration of isotropic, orthotropic and laminated plates according to a higher-order shear deformation theory, J. Sound Vib. 98 (2) (1985) 157–170.
[25] C.W. Bert, M. Malik, Differential quadrature method in computational mechanics: a review, Appl. Mech. Rev. 49 (1996) 1–28.
[26] J. Yuan, K.M. Liew, Effects of vacancy defect reconstruction on the elastic properties of carbon nanotubes, Carbon 47 (6) (2009) 1526–1533.
[27] A.A. El-Barbary, R.H. Telling, C.P. Ewels, M.I. Heggie, P.R. Briddon, Structure and energetics of the vacancy in graphite, Phys. Rev. B 68 (14) (2003) 144107.
[28] G.D. Lee, C.Z. Wang, E. Yoon, N.M. Hwang, D.Y. Kim, K.M. Ho, Diffusion, coalescence, and reconstruction of vacancy defects in graphene layers, Phys. Rev. Lett. 95 (20) (2005) 205501.